Research Article | Vol. 28, No. 21 / 12 October 2020 / Optics Express 31714
Optics EXPRESS

Multi-layer light trapping structures for enhanced solar collection

RAKAN E. ALSAIGH,[1,3] RALF BAUER,[2] AND MARTIN P. J. LAVERY[1,4]

[1]James Watt School of Engineering, University of Glasgow, Glasgow, UK
[2]Department of Electronic and Electrical Engineering, University of Strathclyde, Glasgow, UK
[3]r.alsaigh.1@research.gla.ac.uk
[4]martin.lavery@glasgow.ac.uk

Abstract: Light trapping is a commonly used technique for enhancing the efficiency of solar collection in many photovoltaic (PV) devices. In this paper, we present the design of multi-layer light trapping structures that can potentially be retrofitted, or directly integrated, onto crystalline or amorphous silicon solar panels for enhanced optical collection at normal and extreme angle of incidence. This approach can improve the daily optical collection performance of solar panel with and without internally integrated light trapping structure by up to 7.18% and 159.93%, respectively. These improvements predict an enhancement beyond many research level and commercially deployed light trapping technologies. We further enhance this performance by combining our multi-layer optics with high refractive index materials to achieve a daily optical collection of up to 32.20% beyond leading light trapping structures. Our additive light trapping designs could enable the upgradeability of older PV technologies and can be tailored to optimally operate at unique angular ranges for building exteriors or over a wide range of incidence angle for applications such as unmanned aerial vehicles.

1. Introduction

Solar photovoltaic (PV) continues to transform the global energy economy as the dominant technology to harness solar energy and one of the cheapest routes to supply electricity [1]. One of the main avenues to increase the efficiency of solar devices is the development of light management strategies to improve the utilisation of incident light and power absorption in the thin PV structures. One way to achieve this is through light trapping schemes that enhance power conversion efficiency of PV devices and compensate for any insufficient light absorption [2]. Light trapping schemes have long been explored as a route to increase the light absorption in PV cells and achieve high efficiency solar conversion. This is achieved by enhanced internal coupling efficiency and prolonging the effective path length of light within the solar PV, which improve the photon-electron conversion and therefore improve the power efficiency of the device.

Various light trapping structures and materials have been explored to achieve higher efficiencies, which include antireflective coatings [3], nanowires [4], nanocones [5], triangular or pyramid structures [6], photonic crystal structures [7], plasmonic nanostructures [8], refractive structures [9], random scatterers [10,11], and microlenses [2,12–16]. However, the majority of these structures are fabricated and integrated into the PV device, which can potentially introduce electric defects that induce recombination loss [12,17]. Utilising additive and replaceable structures to trap light is potentially a more desirable approach to avoid the recombination losses and enable future upgrades of older light trapping technologies. Microlens arrays combined with mirrors have been demonstrated as a separate structure for enhanced light trapping [12]. However, such structures rely on precision focusing and have a limited acceptance angle, which is incompatible

#403990 https://doi.org/10.1364/OE.403990
Journal © 2020 Received 4 Aug 2020; revised 6 Sep 2020; accepted 15 Sep 2020; published 6 Oct 2020

Optics EXPRESS

with deployment in autonomous and mobile devices, rooftops and many other non-tracking applications – where a significant share of the global photovoltaic power is produced [18].

Multi-element optical devices are revolutionising the way we control light for many photonics technologies and can be tailored to transform the trajectories of light in a bespoke manner. Recent advances have demonstrated the use of such multi-element optics in the form of a lenslet array for efficient solar collection at extreme angle of incidences [19]. These systems can be a compound of multiple optical elements or the combination of optics with novel materials to achieve multi-layer unconventional control of light. They can also be adapted and tailored to enable common basic solar panels to be efficiently used in various deployment scenarios. The development of such multi-layer additive optical structure that can avoid potential electrical defects and losses, increase the angular acceptance window of additive light trapping structures and offer high efficiencies over a large set of incident angles has the potential to enable future-generation changeable and upgradeable light trapping structures.

In this paper, we present additive multi-layer optical designs that can be retrofitted on top of crystalline or amorphous silicon solar panels to increase their power conversion efficiency through the promotion of light trapping. We highlight two designs that are based on lenslet arrays with wide light incidence field of view capabilities (±80°), which are (1) multi-element lenslet arrays of inverted hemispheric lenses that are periodically arranged and bonded with their curved and flat faces slightly overlapping (Inverted MELA) and (2) multi-element lenslet arrays of hemispheric lenses that are non-uniformly distributed and bonded with their curved faces touching (Non-uniform MELA), see Fig. 1. The multi-layer array nature of these optical designs enables incident light on one lens in the first array to be collected and redirected over a cluster of lenses in the second array, which then spread the rays to have an angular distribution that promotes light trapping within the solar cell. This ray distribution prolongs the average light path length within the solar cell absorber layer, leading to an increase in the optical absorption. Our optical designs (based on N-BK10 glass with $n \approx 1.5$) can be added onto solar panels with and without internally integrated light trapping structures to achieve further increases in path length and absorption probability for both normal and extreme incidences. We explore these designs through modelling the optical power increase (i.e., increase in optical power that can be absorbed by the active layer of the solar cell based on absorption path length statistics) with the addition of each design onto a textured crystalline silicon solar panel and an untextured amorphous silicon solar panel. The ideal optical design will vary based on application, where we predict the optimum MELA design on top of a crystalline silicon solar panel with industry leading integrated light trapping for normal solar incidence deployment is the inverted MELA with an optical collection increase in the active layer of 5.98%. For solar collection over a full day with considerable varying optical incidence, the optimal coupling at equatorial latitudes is achieved by the non-uniform MELA, yielding an optical collection increase of 7.18%. Similarly, for an amorphous silicon solar panel with no integrated light trapping, we expect the optimum design for both normal and full day solar incidences to be the non-uniform MELA, with an optical collection increase of 132.14% and 159.93% at normal incidence and over a full day at equatorial latitudes, respectively. Additionally, we can further reduce the reflection losses and increase the optical gains of these MELA designs by combining the optics with higher refractive index materials. Our models predict that for the use of higher refractive index materials, we could see up to 32.20% and 318.64% increase in the daily solar collection for the crystalline and amorphous silicon solar panel, respectively. The use of this novel optics-material combination does not only help with minimising the intermediate reflection losses, but also aid light coupling and light trapping for a wide range of incident angles. These gains may vary depending on the solar panel technology and we expect these gains to be higher for solar panels with lower power conversion efficiency.

Optics EXPRESS

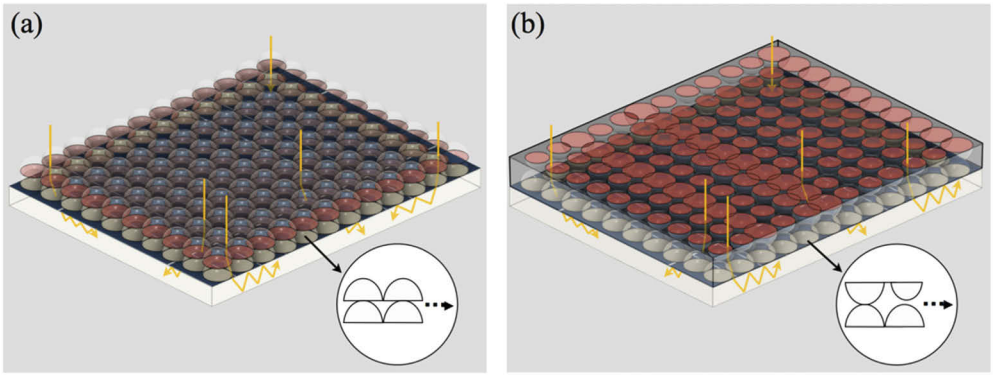

Fig. 1. Illustration of the two multi-layer optical designs. (a) Schematic of an inverted multi-element lenslet array (MELA) integrated onto the top surface of a solar panel. This design is based on 1 mm radius and 1 mm thick hemispheric lenslet arrays arranged with the flat surface of the first array bonded onto the curved surfaces of the second array. (b) Illustration of the non-uniform MELA. The first array in this MELA has lenslets with non-uniform distribution and dimension that were randomised using a Monte Carlo optimisation method. The edges of the arrays in this design are mirrored to further promote light trapping in the solar cell (denoted as a grey box).

2. Multi-layer optics

Figure 1 illustrates the general layout of the multi-layer optical systems we designed as additive light trapping structures, where these designs can simply be retrofitted onto the external pane of solar panels for an enhanced optical performance. The multi-layer lenslet array approach is adopted from recent work outlining a design of two arrays of hemispheric lenses that are bonded together with their curved faces, to be used on top of solar cells to promote light trapping at extreme angles and enable their use in non-tracking deployments. These optical elements build on our previously reported MELA arrangement to produce a wide field of view (±80°) that allows efficient coupling for normally incident light with increased efficiency for rays incidents at high angles of incidence [19]. This previously reported MELA design focused on solar cells with no integrated light trapping structures, limiting the designs compatibility for a broad range of commercially deployed solar panels. Inspired by these early optical designs, a range of redesigned multilayer optical elements are explored that provide additional gains in optical collection when partnered with solar cells containing internally integrated light trapping structures. We outline the performance of several new optical designs that have a non-planar input surface, a Monte-Carlo optimised non-uniform lens profile, and high-refractive index internal layers; where each offer distinctive optical collection enhancements depending on the intended application for the solar cells.

The first of our presented optical system designs reverses the orientation of the top lens array of the original MELA design to remove the planar optical surface with the intension to reduce reflective losses at high input angles, see Figs. 2(a) and 2(b). The hemispheric lenses in both the arrays of our inverted MELA have a 2 mm aperture, a 2 mm focal length, and 2 mm period; providing a uniform array and lens profile that is easy to machine and dimensions that can be readily integrated onto the surface of solar panels without the requirement for micro/nano-scale precise bonding techniques. This lens arrangement provides an effective diffusion of visible and near infrared light for at both near normal incidence angle and extreme angles of incidence that promote total internal reflection in the devices active layer that leads to increased optical collection. This also allows incoming light to be initially focused by first lens array and then

Optics EXPRESS

subsequently defused by a second lens array placed shorter than one focal length away from the first. This enhances the coupling of normally incident light in particular as it promotes the angular spreading of solar radiation. The non-planar optical surface can further reduce reflective losses on the edges of the first array lenses for light incident at particular angles. Such arrangement resolves some of the reflective losses of the previously presented MELA design [19], while providing a similar angular diffusion of light at higher incident angles. Our simulation indicate that this design is particularly useful for near-normal incidence deployment and can be employed for case-specific applications where the solar alignment is predefined or guaranteed, such as tracking-integrated systems.

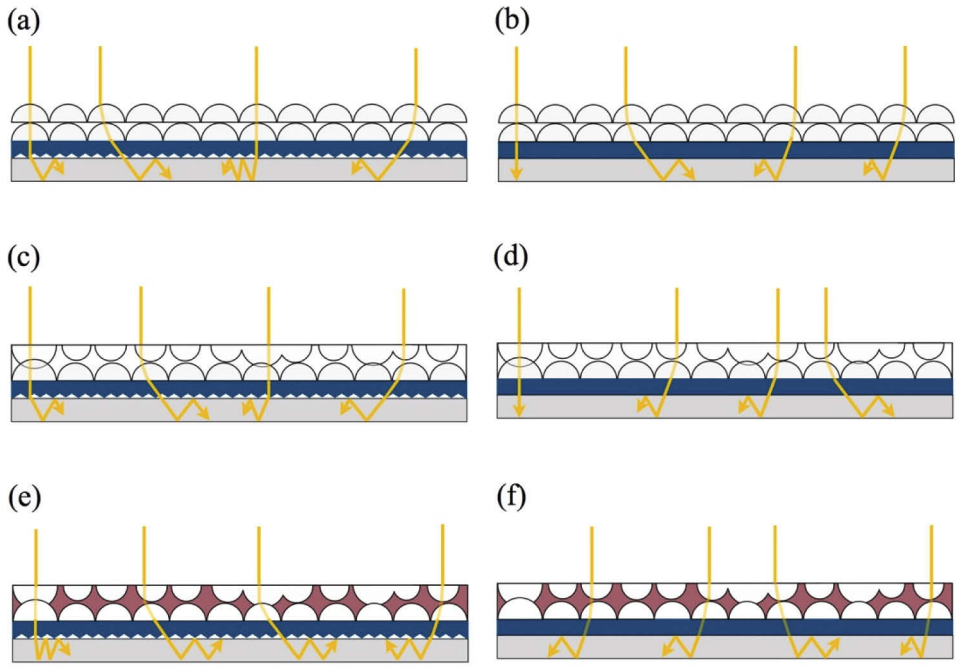

Fig. 2. Cross-section of the multi-element optical designs. (a) A cross-section illustration of the inverted MELA on top of a crystalline silicon solar panel that consists of the crystalline silicon layer (denoted in grey) and encapsulated with polycarbonate cover (denoted in blue). The crystalline silicon cell has integrated front pyramidal light trapping structures partnered with a rear silver reflector (R=97.5%). (b) The inverted MELA cross-section on top of an amorphous silicon solar panel that consists of the amorphous silicon layer (denoted in grey) and encapsulated with glass cover (denoted in blue). The amorphous silicon cell has a rear silver reflector (R=97.5%) but no front integrated light trapping structure. (c) A cross-section illustration of the non-uniform MELA on top of the crystalline silicon solar panel, which also has integrated front pyramidal light trapping structures and a rear silver reflector. (d) The non-uniform MELA cross-section on top of the amorphous silicon solar panel, with integrated rear silver reflector but no front light trapping structure. (e) The cross-section illustrates the non-uniform MELA, with deposited high refractive index material (red) within the multi-elements instead of air, on top of the crystalline silicon solar panel with the integrated front pyramidal light trapping structure and a rear silver reflector. (f) Illustration of the cross-section of the non-uniform MELA, with deposited high refractive index material (red) within the multi-elements instead of air, on top of the amorphous silicon solar panel with the integrated rear silver reflector but with no front pyramidal light trapping structure.

Optics EXPRESS

Inspired by the active debate between the use of periodic and random light trapping structures [20], we investigated a second design that uses a multi-layer lenslet array approach with a non-uniform lens distribution and dimension to examine if moving away from uniform arrays could lead to an improvement in light collection. This non-uniform MELA has two arrays of short-focal length hemispheric lenses that are distributed and arranged non-uniformly and bonded together with their curved faces, see Figs. 2(c) and 2(d). We utilised a gradient-free Monte Carlo optimisation solver in Comsol Multiphysics to randomise the design by maximising the optical power collected by the solar cell active layer at normal incident, with the option of mirroring the edges of the optical arrays. The Monte Carlo solver was specifically exploited as it utilises randomly generated sample points with a uniform distribution to look for the optimum point within a specific range of values that we defined based on the manufacturability of lenses [21]. Each lens diameter was initially set to 2 mm and the specific diameter range was varied between ±0.4 mm with a position displacement of ±0.2 mm. The final cross section shows that the minimum and maximum lens radius is between 0.81 mm and 1.19 mm and the period between each lens to its neighbouring lens varies with minimum and maximum values of 1.63 mm and 2.22 mm, respectively. Figure 2(c) and 2(d) detail the final cross-section of the non-uniform MELA, where the maximum performance is found to be when the edges of the arrays are finished with a reflective coating, where this side mirror arrangement is illustrated as a grey box in Fig. 1. Although this design was optimised for normal incidence, the angular performance is found to outperform the inverted MELA and other industry integrated light trapping structures. This superiority is expected to be due to the numerical derivation of the optimum lens position and radius of each lens in the upper array to collect light in a manner that achieves maximum coupling and minimum losses. This performance is predicted to be scalable for larger solar modules, where the non-uniform lens distribution can be replicated periodically to yield a similar optical behaviour over a wider surface area. Similarly, we expect similar performance if the lens diameter is proportionally changed with the panel surface area, while taking into consideration the subsequent changes in the thickness and separation of the hemispheric lens. Generally, this method can also be used to develop and tailor other lens distributions designed for various use-cases or case-specific applications that optimally operate at a desire angular range or at a fixed incidence for applications such as unmanned aerial vehicle or building exteriors. The dimensions of the lens structures should be easily manufactured with traditional optical machining, injection moulding or 3D printing.

3. System performance

We evaluate the light trapping performance of these structures by modelling the solar collection within the photovoltaic cell with and without our retrofitted optical design, where the solar collection is defined as the fraction of optical power incident on the optical elements that can be absorbed by the active layer of the solar cell. The optical simulations were numerically performed using Comsol Multiphysics with our optical designs integrated onto the top surface of the cSi and aSi devices, where each device is structured with an encapsulation material on top of the silicon layers as detailed Fig. 2. These models employ a 1000 W/m^2 plane wave illumination that is released onto the total input aperture of our structures and subsequently compute the geometrical optical power absorption within the solar cell absorber layer for rays with a power density equivalent to or greater than 1 mW/m^2 over incident angles of 0°-80° in a 2° step. These models consider the transmission and reflection at each material boundary with monitors enclosing the devices to detect the rays that enter and leave the device, while computing the geometrical optical ray power that can be absorbed within the solar cell absorber layer. The geometrical optical absorption was computed by defining the conversion efficiency for a single normal light bounce within the active layer based on our reference commercial silicon solar cells and then calculating for any additional light bounces for both the textured PV and

Optics EXPRESS

MELA integrated designs. This geometrical analysis also takes into consideration the path length dependent power absorption to fully account for the additional angle dependent light trapping. Using this model, each design was simulated on top of two different types of commercial silicon PVs; a 25%-efficient monocrystalline silicon solar panel (IXYS, KXOB25-14X1F) and a 3.58%-efficient amorphous silicon solar panel (Sanyo, AM-5610). The numerically simulated structure of the crystalline silicon device consists of the crystalline silicon layers (denoted in grey in Figs. 2(a), 2(c), and 2(e)) and polycarbonate encapsulant (denoted in blue in Figs. 2(a), 2(c) and 2(e)). For the amorphous silicon device, the structure consists of the amorphous silicon layers (denoted in grey in Figs. 2(b), 2(d), and 2(f)) and glass encapsulant (denoted in blue in Figs. 2(b), 2(d), and 2(f)). These encapsulations are typically used to protect the solar cells and improve their reliability and durability [22], where the encapsulating material in this work is determined based on the datasheet of the example cSi and aSi panels. To match the typical alkaline texturing process of commercial cSi solar panels, we use front pyramidal textures with a pitch of 10 μm and angle of 54.7° [23]. For both types of silicon solar panels, the absorber layer was back-reflected with a rear silver reflector (R = 97.5%). These specific silicon-based solar panels were chosen since crystalline silicon is dominating more than 90% of the PV global market [24] and amorphous silicon is considered the most common form of thin-film photovoltaic cells [25]. These devices were also used to show the effect of our designs on different technologies that have a high efficiency solar cell with integrated light trapping and a low efficiency solar cell with no light-trapping structure and demonstrate how the optical gain would vary between the two. These gains are directly compared and referenced to as-commercially sold solar panels prior to the integration of our MELA designs.

Figures 3(a) and 3(b) displays the optical performance for our optimised MELA designs together with that for the as commercially-sold reference solar panels over 80° incidence angles in a 2° step. These results predict that the addition of our non-uniform MELA into a crystalline silicon solar panel with industry light trapping structure would yield an optical collection gain of up to 7.18% over incident angles of 80° at equatorial latitudes, see Fig. 3(a). Although this non-uniform MELA showed the highest optical gain in the crystalline silicon comparison over a full day, the inverted MELA is expected to show the peak optical collection performance for normal incidence deployments of 5.98%, see Fig. 3(a). These designs also show a smooth daily optical collection behaviour, aided by their wide field of view and initial spread of rays as the light enters the solar panel, where the removal of these elements result in angle-dependent fluctuations in the optical collection of the textured PV, see Fig. 3(a). These fluctuations are expected to be due to the fact that industrial pyramidal texturing is designed for near normal operation and not optimised for a wide range of acceptance angles, yielding a surface structure that is sensitive to angular rotation. The addition of the non-uniform MELA onto an amorphous silicon panel with no integrated light trapping structures would result in an optimum optical gain for both normal and full-day incidences at equatorial latitudes of 132.14% and 159.93%, respectively, see Fig. 3(b). The enhancement factors in solar collection for adding these MELA designs on the textured and flat solar PVs are shown in Fig. 7 in the Appendix. Also, complete tables with solar collection increases and theoretical power conversion efficiencies are shown in Table 1 and Table 2, respectively.

Based on these solar collection results and using the short circuit current density (J_{sc}) and the open circuit voltage (V_{oc}) of the two commercial panels, we modelled the expected J_{sc} and V_{oc} for the addition of optimum MELA designs at normal incidence for the two types of silicon solar panels, as shown in Figs. 3(c) and 3(d). For the crystalline silicon panel, we expect the J_{sc} to improve from 41.359 mA/cm^2 to 41.626 mA/cm^2 and the V_{oc} from 0.690 V to 0.701 V when the Inverted MELA is used. We also expect these J_{sc} and V_{oc} to improve to 41.431 mA/cm^2 and 0.693 V for the addition of the non-uniform MELA, respectively. Although these results yield minor electrical increases for normal incidence, we will show that they can be further improved

Optics EXPRESS

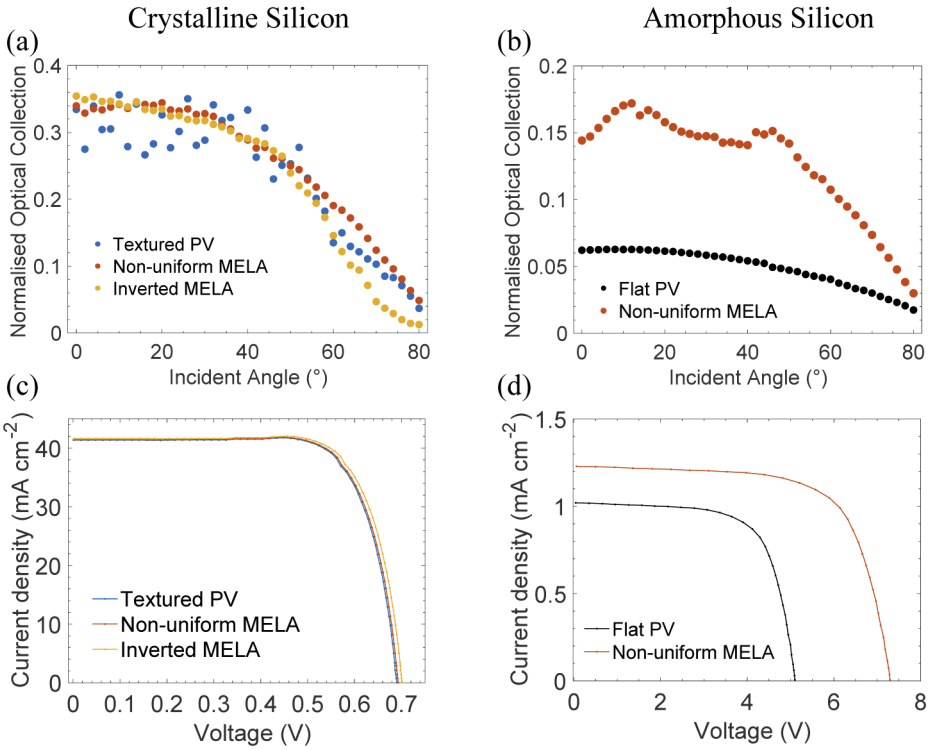

Fig. 3. Simulated system performance with and without the MELA designs. (a) Solar collection normalised over the incident optical power, showing the geometrical solar power collected by a 25%-efficient commercial crystalline silicon device (denoted as Textured PV. Manufacturer: IXYS, KXOB25-14X1F) and those for the addition of our non-uniform and inverted MELAs over 0°-80° incidences. (b) Solar collection normalised over the incident optical power, displaying the geometrical solar power collected by a 3.58%-efficient commercial amorphous silicon device (denoted as Flat PV. Manufacturer: Sanyo, AM-5610) and that for the addition of our non-uniform MELA over 0°-80° incidences. (c) IV curve of the commercial crystalline silicon panel and the simulated IV curves for the addition of our non-uniform and inverted MELAs at normal incidences. (d) IV curve of the commercial amorphous silicon panel and the simulated IV curve for the addition of our non-uniform MELA at normal incidences.

Table 1. Percentage optical gain or loss for the addition of the inverted, non-uniform MELA and non-uniform MELA with diamond and polymer on the crystalline and amorphous silicon solar panels for normal and full-day incidences at equatorial latitudes.

Optical Element	Optical Increase (%)			
	Crystalline Silicon		Amorphous Silicon	
	Normal Incidence	0° – 80° Incidences	Normal Incidence	0° – 80° Incidence
Inverted MELA	5.98	-0.71	111.24	84.98
Non-uniform MELA	1.60	7.18	132.14	159.93
Non-uniform MELA, Polymer	16.33	17.74	132.33	129.61
Non-uniform MELA, Diamond	38.36	32.20	366.73	318.64

Optics EXPRESS

Table 2. Expected theoretical power conversion efficiency of the specific simulated solar cells with and without our MELA designs for normal incidences at equatorial latitudes.

Solar Panel	Theoretical Power Conversion Efficiency				
	Without MELA	Inverted MELA	Non-uniform MELA	Non-uniform MELA, Polymer	Non-uniform MELA, Diamond
Crystalline Silicon	25.0%	25.5%	25.1%	26.5%	28.4%
Amorphous Silicon	3.5%	5.8%	6.1%	6.1%	10.0%

using a multi-material layer method. Similarly, we predict the J_{sc} to increase from 1.02 mA/cm^2 to 1.229 mA/cm^2 and the V_{oc} from 5.1 V to 7.294 V for the amorphous silicon panel when using the non-uniform MELA. It should be noted that such gains are for crystalline silicon with front texture and rear mirror and amorphous silicon with front flat surface and rear mirror, which could vary based on the specific light trapping structure and efficiency of the panels being used. Generally, these results show that our additive light trapping systems would have higher gain for a lower efficiency panel, as high efficiency panels already have a higher absorption probability due to their integrated light-trapping surface, resulting in a smaller room for collection enhancement. These electrical increases are modelled for normal incidence, where a cumulative daily incidence is expected to yield a higher electrical generation.

Based on the multi-layer nature of our designs that inherently include a material variation within the element, we further investigated the effect of combining the optics with materials that have refractive indices higher than air to minimise parasitic internal reflections and achieve unconventional control of light. The use of such material combinations is not only an approach to control light trapping, it is also demonstrated to help mitigate chromatic dispersion in a manner similar to an achromatic doublet [18]. We explored this variance in our designs by depositing the material in place of the air gaps within the non-uniform MELA as illustrated in Figs. 2(e) and 2(f). We modelled this combination using a commonly used low-dispersion N-BK10 glass ($n \approx 1.5$) for the optics together with a range of materials with refractive indices ranging between $n = 1$ to $n = 2.4$, see Fig. 4. These results predict that when the material-combined element is used with the crystalline silicon solar panel a drop in optical efficiency will occur near $n = 1.4$ then it will increase with the refractive index, see Fig. 4(a). This drop is expected to be caused by the material variance between the optical glass and the PV polycarbonate encapsulant. For the amorphous silicon solar panel, the optical efficiency drops between $n = 1$ and $1 \approx 1.7$, with no gain at $n = 1.5$, see Fig. 4(b). This is also predicted to be due to the fact that for a glass-encapsulated amorphous PV, the glass MELA will be equivalent to a plain block at $n = 1.5$ and hence equivalent to the panel prior to the element integration. Examples of potential materials with refractive indices higher than glass are certain polymer compounds ($n \approx 1.725$) [26], N-LASF31A glass ($n \approx 1.88$) [27] and diamond ($n \approx 2.4$) [28]. We use these materials as examples since they are transparent in the visible and NIR ranges and have a low refractive index dispersion over the wavelength range absorbed by the crystalline silicon ($300\ \text{nm} < \lambda < 1200\ \text{nm}$) and amorphous silicon ($300\ \text{nm} < \lambda < 800\ \text{nm}$) PVs. However, other broadband transparent materials with refractive indices in this range could also be suitable with our non-uniform MELA. This model expects the optimum optical collection by the solar cell to occur when the glass is combined with diamond or a material with similar properties as diamond.

We further investigated the use of diamond and polymer as high refractive index materials since diamond shows the optimum optical collection and polymer is the easiest material to deposit within the optical element. We modelled the solar coupling for the addition of our material-combined non-uniform MELA onto the reference solar panels over 80° incidence angles in a 2° step. Similar to the previously defined optical simulation, this model also employs a 1000

Optics EXPRESS

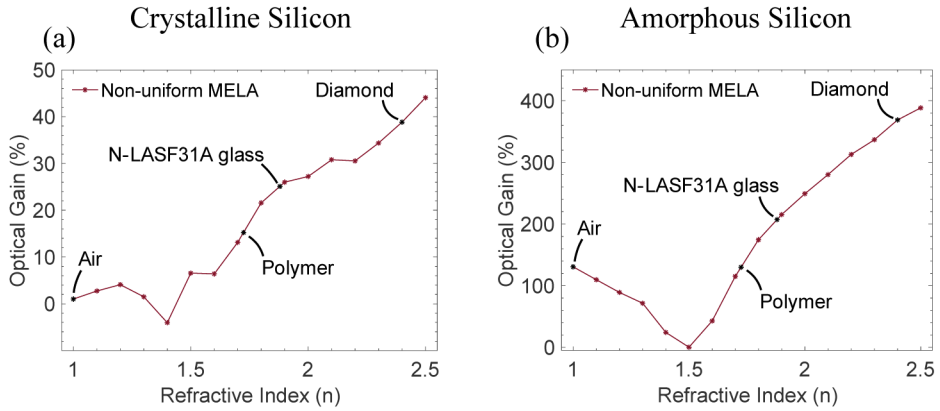

Fig. 4. Simulated optical gain for varying the material within the multi-layer optical element. (a) Percentage optical gain for adding the non-uniform MELA onto the crystalline silicon solar cell as a function of the refractive index of the material within the non-uniform MELA for normal incidence. This plot denotes the proposed materials with their expected gains. The example textured c-Si solar panel is encapsulated with polycarbonate material ($n \approx 1.57$) according to the device datasheet, creating a material variance at the MELA integration boundary that explains the drop in optical efficiency below zero at n=1.4 and the increase near 1.5. It is important to note that when a filler material has a refractive index equivalent to the optics we used, the optical element will act as a plain block with side mirrors. (b) Percentage solar increase for adding the non-uniform MELA onto the amorphous silicon solar cell as a function of the refractive index of the material within the non-uniform MELA for normal incidence. This plot denotes the proposed materials with their expected gains. The example untextured a-Si solar panel is encapsulated with glass material according to the device datasheet, making the MELA equivalent to a plain block at $n = 1.5$ and hence equivalent to the panel prior to the MELA integration.

W/m^2 plane wave illumination that is released onto the total input aperture of the non-uniform MELA and the geometrical optical power absorption within the solar cell absorber layer for rays with a power density equivalent to or greater than 1 mW/m^2 is then computed. However, for this material-combined simulation, the airgap regions within the lens arrays were filled with polymer compound ($n \approx 1.725$) and diamond ($n \approx 2.4$) as illustrated in red in Figs. 2(e) and 2(f). We found that the addition of this non-uniform MELA with diamond onto the crystalline silicon solar panel with integrated light trapping would result in optimum optical increase for both normal and full-day incidences at equatorial latitudes of up to 38.4% and 32.2%, respectively, see Fig. 5(a). This model also shows that adding the non-uniform MELA with polymer onto the crystalline silicon solar panel yields optical increases of 16.3% and 17.7% for normal and full-day incidences at equatorial latitude, respectively, see Fig. 5(a). The use of this compound polymer with our non-uniform MELA provides an optical collection that is always higher than the textured PV, which is a considerable improvement above its air counterpart. Similarly, the addition of this non-uniform MELA with diamond on top of the amorphous silicon solar panel with no integrated light trapping structure would yield optimum solar increase for both normal and full-day incidences at equatorial latitudes of up to 366.73% and 318.64%, respectively, see Fig. 5(b). It is also expected by adding the non-uniform MELA with polymer onto the amorphous silicon solar panel, optical gains of 132.33% and 129.61% would be achieved for normal and full-day incidences at equatorial latitudes, respectively. Although the use of high refractive index materials has mostly shown optical increases over their air counterparts, our model predicts that using polymer in place of air within the non-uniform MELA on top of the amorphous silicon

Optics EXPRESS

solar panel would reduce the overall daily gain from 159.93% to 129.61%. This reduction is expected to be due to the slight material variance between the optical element (glass), panel encapsulant (glass) and deposited polymer; resulting in a smaller diffusion of light, structural behaviour and light trapping in comparison to the air counterpart. For these solar increases and using the crystalline silicon panel, we predict the J_{sc} and V_{oc} to improve to 43.069 mA/cm^2 and 0.754 V for the non-uniform MELA with diamond, as well as to 42.087 mA/cm2 and 0.720 V for the non-uniform MELA with polymer, respectively. We also expect the J_{sc} and V_{oc} to increase to 1.601 mA/cm^2 and 9.114 V for the non-uniform MELA with diamond, as well as to 1.229 mA/cm^2 and 7.296 V for the non-uniform MELA with polymer for the amorphous silicon panel, respectively. Generally, these optical gains confirm that by combining optical elements with novel materials, one can further improve the light control and further promote light trapping, and hence enhance the absorption of the light beyond their air coupled counterparts. Although combining these designs with high refractive index materials is more complex to manufacture,

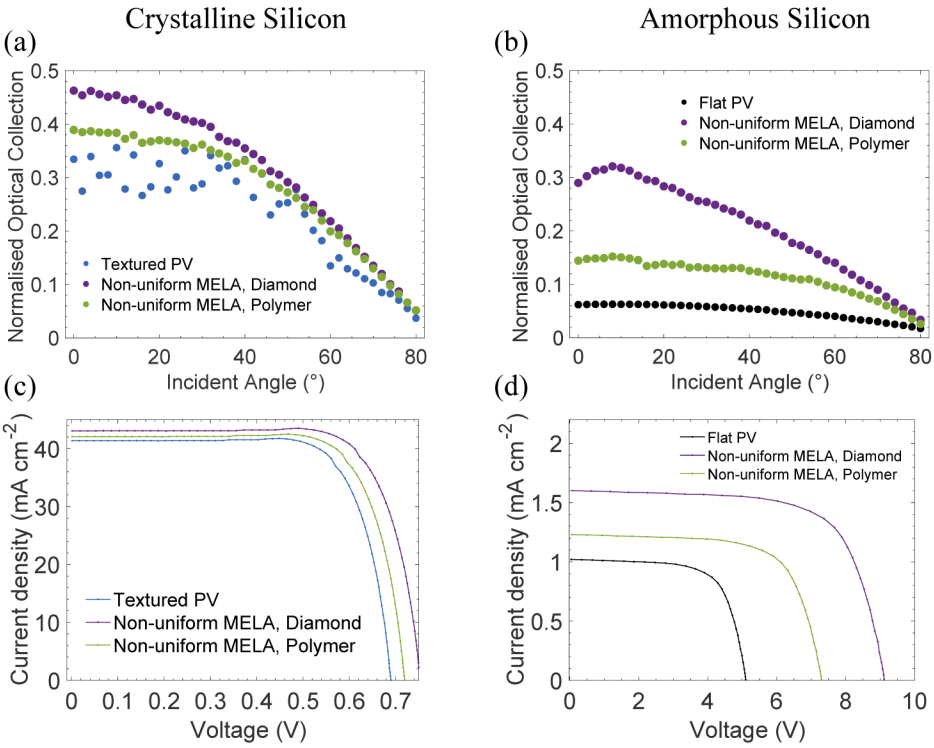

Fig. 5. Simulated system performance with high refractive index materials. (a) Normalised solar collection for the textured crystalline silicon solar cell and for the addition of our non-uniform MELA when diamond and polymer are deposited in place of the air gaps over 0°-80° incidences. (b) Normalised solar collection for the flat amorphous silicon solar cell and for the addition of our non-uniform MELA when diamond and polymer are deposited in place of the air gaps over 0°-80° incidences. (c) IV curve of the 25%-efficient commercial crystalline silicon panel (IXYS, KXOB25-14X1F) and the expected IV curves for the addition of our non-uniform MELA when diamond and polymer are deposited in place of the air gaps at normal incidences. (d) IV curve of the 3.58%-efficient commercial amorphous silicon (Sanyo, AM-5610) and the expected IV curves for the addition of our non-uniform MELA when diamond and polymer are deposited in place of the air gaps at normal incidences.

Optics EXPRESS

their improved performance and enhanced light absorption might be of interest for many high efficiency applications.

Further, we investigated the effect of the solar panel efficiency on the optical gain produced for the addition of our non-uniform MELA, which can show the benefit of our MELA design for other solar panel technologies and generalise our study for a wide range of devices. Figure 6 shows the percentage optical gain for the addition of our non-uniform MELA on the crystalline and amorphous silicon solar panels with power absorption efficiencies ranging between 12%-29.5% and 2.5%-15% in a step of 0.5% at normal incidence, respectively. This simulation was performed using the previously defined geometrical optical absorption with the only difference that the incident angle of the input beam here was fixed at normal and the solar cells efficiency was swept over a range of efficiencies to vary the panel power conversion efficiency. This efficiency sweep was performed by varying the absorption factor that defines the conversion efficiency for a single normal light bounce within the absorber layer and subsequently compute the increase in optical power that can be absorbed for rays with power density equivalent to or greater than 1 mW/m^2. These efficiency ranges were determined to encompass the minimum average efficiency for commercial devices (see [29] for crystalline silicon and supplementary material in [19] for amorphous silicon) and the theoretical efficiency limit for each silicon technology (see [30] for crystalline silicon and [31] for amorphous silicon). Both results predict that the optical gain decreases as the panel efficiency increases. Although our light trapping approach would not result in significant further optical collection improvements when retrofitted onto solar panels that readily employ perfect light trapping structures, our approach could potentially benefit many other solar panel systems that suffer optical losses including many top performing c-Si devices [32]. Additionally, our additive approach demonstrates a compelling route for improved performance over extreme angles, as most integrated light trapping structures are optimised for normal incidences. This is expected to be due to the ability of high efficiency cells to absorb the majority of the incident light and yield full light absorption in the first few light bounces, which removes the further reliance on light trapping structures to aid and increase the optical path length, and hence removes the need to compensate for insufficient light absorption for normal incidence. However, our additive multi-layer approach and designs are still expected to collect light over a wide range of angles; which subsequently improves their light trapping and

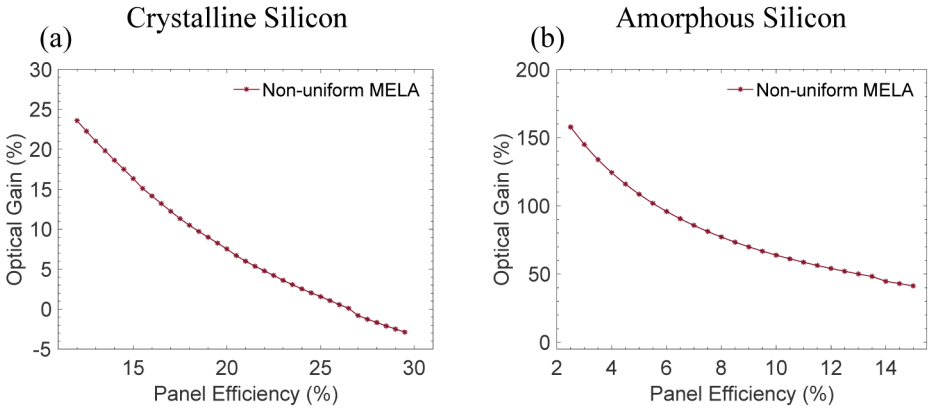

Fig. 6. Simulated expected optical gain as a function of panel power conversion efficiency. (a) Percentage optical gain for adding the non-uniform MELA onto a crystalline silicon solar panel with different panel power conversion efficiency at normal incidence. (b) Percentage optical gain for adding the non-uniform MELA onto an amorphous silicon solar panel with different panel power conversion efficiency at normal incidence.

Optics EXPRESS

absorption for non-normal, extreme and daily incidences. It is also important to note that the non-uniform MELA will always produce optical gain for amorphous silicon panels even at their theoretical efficiency limit.

4. Conclusion

In this paper, we have designed additive and replaceable multi-layer lenslet array (MELA) structures that can be readily retrofitted onto crystalline or amorphous silicon solar panel for enhanced light trapping and solar collection. Our designs can be used on top of solar panels with and without internally integrated light trapping structures and increase their solar collection at normal and high angles of incidence. We outlined two MELA optical designs (1) Inverted MELA and (2) Non-uniform MELA with two different silicon technologies, a textured crystalline silicon solar panel and an untextured amorphous silicon solar panel. We note the optimum design for each silicon technology and deployment alignments, where the non-uniform MELA is found to be the dominating candidate. Additionally, we combined the non-uniform MELA with high refractive index materials to improve the optical collection of the solar cells and expect an optimal performance when the optics is combined with diamond or diamond-like materials. The optical improvements achieved for our designs above the reference solar panels were modelled for the additional geometrical optical power absorbed by the solar cell active layer for the further promoted light trapping. It is important to note that these optical gain subsequently lowers the optical losses of the solar device, which is one of the three main losses that can be improved for the device to approach the efficiency limit of solar cells [32]. This additive MELA approach does not only help overcome some limitations of internal light trapping structures; but also provides a compatible solution for commercial and future-generation solar devices, which can be used to replace or upgrade older technologies and enable solar cell performance improvements in various use cases such as autonomous devices, mobile vehicles, rooftops and future telecommunication networks [33].

Appendix 1: Optical enhancement

Figures 7(a) and 7(b) outline the enhancement factor in optical collection for the inverted and non-uniform MELA as a function of incident angle over the textured cSi and flat aSi PVs presented in Fig. 3, respectively. Similarly, Figs. 7(c) and 7(d) present the optical enhancement factor for the non-uniform MELA when diamond and polymer are deposited in place of the air gaps over the textured cSi and flat aSi PVs presented in Fig. 5, respectively.

Optics EXPRESS

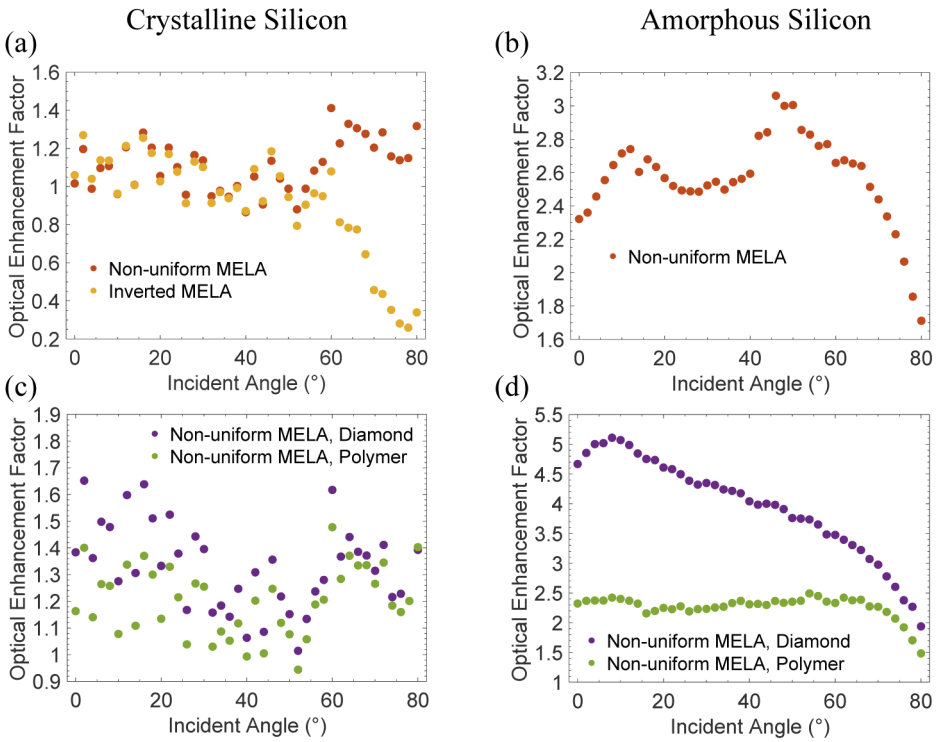

Fig. 7. Optical enhancement factor for the addition of the MELA designs. (a) Enhancement factor in solar collection as a function of incident angle for the addition of the non-uniform and inverted MELA over the crystalline silicon device. (b) Enhancement factor in solar collection as a function of incident angle for the addition of the non-uniform MELA over the amorphous silicon device. (c) Enhancement factor in solar collection for the addition of the diamond and polymer deposited non-uniform MELA over the crystalline silicon device. (d) Enhancement factor in solar collection for the addition of the diamond and polymer deposited non-uniform MELA over the amorphous silicon device.

Appendix 2: Electric field intensity of the non-uniform MELA

Figure 8 illustrates the spatial electric field intensity through the non-uniform MELA with free-space and silicon propagation before and after the MELA, respectively. The field was propagated at a fixed wavelength (660 nm) using a beam envelope numerical simulation for a simplified illustration of the light distributions and effects produced by our design. For this visualization, the incident beam was matched into a free-space boundary with a 1 V/m input envelope that transitions through the non-uniform MELA and the flat silicon layer boundaries.

Optics EXPRESS

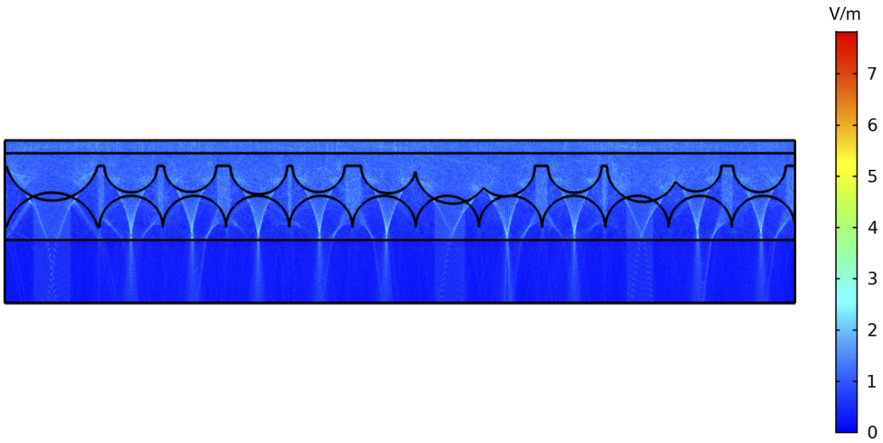

Fig. 8. Electric field intensity for the non-uniform MELA. The electric field is propagated through free-space (top) before coupling into the non-uniform MELA (middle) that is bonded to a flat silicon layer (bottom), where the thickness of this Si layer is extended for illustration purposes.

Funding

Engineering and Physical Sciences Research Council (N032853/1); Ministry of Education – Kingdom of Saudi Arabi; Saudi Arabia Cultural Bureau in London; Royal Academy of Engineering; H2020 Future and Emerging Technologies (Super-Pixels grant number 829116).

Acknowledgments

The authors would like to thank Dr. Johannes Courtial and Prof. Nikolaj Gadegaard for useful discussions.

Disclosures

The authors declare no competing interests.

References

1. M. A. Green, "How Did Solar Cells Get So Cheap?" Joule **3**(3), 631–633 (2019).
2. C. Cho and J.-Y. Lee, "Multi-scale and angular analysis of ray-optical light trapping schemes in thin-film solar cells: Micro lens array, V-shaped configuration, and double parabolic trapper," Opt. Express **21**(S2), A276–A284 (2013).
3. P. M. Voroshilov, C. R. Simovski, P. A. Belov, and A. S. Shalin, "Light-trapping and antireflective coatings for amorphous Si-based thin film solar cells," J. Appl. Phys. **117**(20), 203101 (2015).
4. E. Garnett and P. Yang, "Light trapping in silicon nanowire solar cells," Nano Lett. **10**(3), 1082–1087 (2010).
5. K. X. Wang, Z. Yu, V. Liu, Y. Cui, and S. Fan, "Absorption enhancement in ultrathin crystalline silicon solar cells with antireflection and light-trapping nanocone gratings," Nano Lett. **12**(3), 1616–1619 (2012).
6. R. Dewan, M. Marinkovic, R. Noriega, S. Phadke, A. Salleo, and D. Knipp, "Light trapping in thin-film silicon solar cells with submicron surface texture," Opt. Express **17**(25), 23058–23065 (2009).
7. P. Bermel, C. Luo, L. Zeng, L. C. Kimerling, and J. D. Joannopoulos, "Improving thin-film crystalline silicon solar cell efficiencies with photonic crystals," Opt. Express **15**(25), 16986–17000 (2007).
8. K. Aydin, V. E. Ferry, R. M. Briggs, and H. A. Atwater, "Broadband polarization-independent resonant light absorption using ultrathin plasmonic super absorbers," Nat. Commun. **2**(1), 517 (2011).
9. S. Esiner, T. Bus, M. M. Wienk, K. Hermans, and R. A. J. Janssen, "Quantification and validation of the efficiency enhancement reached by application of a retroreflective light trapping texture on a polymer solar cell," Adv. Energy Mater. **3**(8), 1013–1017 (2013).
10. Z. Hu, J. Zhang, and Y. Zhao, "Effect of textured electrodes with light-trapping on performance of polymer solar cells," J. Appl. Phys. **111**(10), 104516 (2012).

Optics EXPRESS

11. S. Manzoor, Z. J. Yu, A. Ali, W. Ali, K. A. Bush, A. F. Palmstrom, S. F. Bent, M. D. McGehee, and Z. C. Holman, "Improved light management in planar silicon and perovskite solar cells using PDMS scattering layer," Sol. Energy Mater. Sol. Cells **173**, 59–65 (2017).
12. K. Tvingstedt, S. Dal Zilio, O. Inganäs, and M. Tormen, "Trapping light with micro lenses in thin film organic photovoltaic cells," Opt. Express **16**(26), 21608 (2008).
13. S. D. Zilio, K. Tvingstedt, O. Inganäs, and M. Tormen, "Fabrication of a light trapping system for organic solar cells," Microelectron. Eng. **86**(4-6), 1150–1154 (2009).
14. Y. Chen, M. Elshobaki, Z. Ye, J. M. Park, M. A. Noack, K. M. Ho, and S. Chaudhary, "Microlens array induced light absorption enhancement in polymer solar cells," Phys. Chem. Chem. Phys. **15**(12), 4297–4302 (2013).
15. A. Peer, R. Biswas, J.-M. Park, R. Shinar, and J. Shinar, "Light management in perovskite solar cells and organic LEDs with microlens arrays," Opt. Express **25**(9), 10704 (2017).
16. A. Peer and R. Biswas, "Nanophotonic Organic Solar Cell Architecture for Advanced Light Trapping with Dual Photonic Crystals," ACS Photonics **1**(9), 840–847 (2014).
17. Z. Tang, W. Tress, and O. Inganäs, "Light trapping in thin film organic solar cells," Mater. Today **17**(8), 389–396 (2014).
18. J. S. Price, A. J. Grede, B. Wang, M. V. Lipski, B. Fisher, K.-T. Lee, J. He, G. S. Brulo, X. Ma, S. Burroughs, C. D. Rahn, R. G. Nuzzo, J. A. Rogers, and N. C. Giebink, "High-concentration planar microtracking photovoltaic system exceeding 30% efficiency," Nat. Energy **2**(8), 17113 (2017).
19. R. E. Alsaigh, R. Bauer, and M. P. J. Lavery, "Multi-element lenslet array for efficient solar collection at extreme angles of incidence," Sci. Rep. **10**(1), 8741 (2020).
20. C. Battaglia, C. M. Hsu, K. Söderström, J. Escarré, F. J. Haug, M. Charrière, M. Boccard, M. Despeisse, D. T. L. Alexander, M. Cantoni, Y. Cui, and C. Ballif, "Light trapping in solar cells: Can periodic beat random?" ACS Nano **6**(3), 2790–2797 (2012).
21. "Optimization Module User's Guide," COMSOL Multiphysics® 78 (2018).
22. C. Peike, C. Peike, I. Hädrich, K. Weiß, I. Dürr, and F. Ise, "Overview of PV module encapsulation materials," Photovoltaics Int. **22**, 85–92 (2013).
23. M. C. Raval and S. Madugula Reddy, "Industrial Silicon Solar Cells," in *Solar Cells*, E. Nayeripour, Mansouri Majid, and Waffenschmidt Mahdi, eds. (IntechOpen, 2019).
24. L. C. Andreani, A. Bozzola, P. Kowalczewski, M. Liscidini, and L. Redorici, "Silicon solar cells: Toward the efficiency limits," Adv. Phys.: X **4**(1), 1548305 (2019).
25. "Photovoltaics: Characterizing Thin Film Solar Cells," http://sci-soft.com/resources/application-notes/photovoltaics-characterizing-thin-film-solar-cells/.
26. H. Jiang, X. Pan, N. Li, Z. Zhang, J. Zhu, and X. Zhu, "Selenide-containing high refractive index polymer material with adjustable refractive index and Abbe's number," React. Funct. Polym. **111**, 1–6 (2017).
27. Schott, "N-LASF31A Data Sheet. (2014)," https://shop.schott.com/advanced_optics/Products/Optical-Glass/Optical-Glass/Lanthanum-Dense-Flint/N-LASF31A/c/optical-glass/glass-N-LASF31A.
28. H. R. Phillip and E. A. Taft, "Kramers-Kronig Analysis of Reflectance Data for Diamond," Phys. Rev. **136**(5A), A1445–A1448 (1964).
29. S. Philipps and W. Warmuth, "Photovoltaics Report 2019.," Fraunhofer ISE PSE Conf. Consult. GmbH 7 (2019).
30. A. Richter, M. Hermle, and S. W. Glunz, "Reassessment of the limiting efficiency for crystalline silicon solar cells," IEEE J. Photovoltaics **3**(4), 1184–1191 (2013).
31. D. E. Carlson and C. R. Wronski, "Amorphous silicon solar cell," Appl. Phys. Lett. **28**(11), 671–673 (1976).
32. K. Yoshikawa, H. Kawasaki, W. Yoshida, T. Irie, K. Konishi, K. Nakano, T. Uto, D. Adachi, M. Kanematsu, H. Uzu, and K. Yamamoto, "Silicon heterojunction solar cell with interdigitated back contacts for a photoconversion efficiency over 26%," Nat. Energy **2**(5), 17032 (2017).
33. M. P. J. Lavery, M. M. Abadi, R. Bauer, G. Brambilla, L. Cheng, M. A. Cox, A. Dudley, A. D. Ellis, N. K. Fontaine, A. E. Kelly, C. Marquardt, S. Matlhane, B. Ndagano, F. Petruccione, R. Slavík, F. Romanato, C. Rosales-Guzmán, F. S. Roux, K. Roux, J. Wang, and A. Forbes, "Tackling Africa's digital divide," Nat. Photonics **12**(5), 249–252 (2018).